Site-Specific Biochemical Functionalization along the Height of Vertically Aligned Carbon Nanofiber Arrays

Timothy E. McKnight,*[,†,‡] Chorthip Peeraphatdit,[§] Stephen W. Jones,[||] Jason D. Fowlkes,[‡,⊥] Benjamin L. Fletcher,[‡,⊥] Kate L. Klein,[‡,⊥] Anatoli V. Melechko,[‡,⊥] Mitchel J. Doktycz,[#] and Michael L. Simpson[‡,⊥]

Monolithic Systems Development Group, Molecular Scale Engineering and Nanoscale Technologies Research Group, and Biological and Nanoscale Systems Group, Oak Ridge National Laboratory, P.O. Box 2008, Oak Ridge, Tennessee 37831, Lawrence University, P.O. Box 559, Appleton, Wisconsin 54912, Earlham College, 801 National Road West, Richmond, Indiana 47374, and Materials Science and Engineering Department, University of Tennessee, Knoxville, Tennessee 37996

Received December 4, 2005. Revised Manuscript Received April 19, 2006

Flexible strategies for the biochemical functionalization of synthetic nanoscale materials can enhance their impact upon a broader range of devices and applications. Here we report approaches for the heterogeneous functionalization of vertically aligned carbon nanofibers, a nanostructured material increasingly used to provide nanoscale components in microfabricated devices. Photoresist blocking strategies are developed for site-specific physical, chemical, and electrochemical functionalization of nanofiber arrays both spatially across regions of the device as well as along the length of the vertical nanofibers. These approaches are explored for the functionalization of nanofiber surfaces with gold, conductive polymers, and DNA and for the biotinylation and subsequent capture of active enzyme- and quantum-dot-conjugated (strept)avidins. Functionalizations are visualized with both fluorescent and electron microscopy and characterized using dye and enzyme assays.

Background

Vertically aligned carbon nanofibers (VACNFs) continue to gain interest as a novel, high aspect ratio, nanostructured material that may be readily integrated into practical devices using the conventional tools of microfabrication. The incorporation of VACNFs as a nanostructured material into multiscale devices has often enhanced the performance of the combined system. For example, a fluorescence-based indicator of biomolecular recognition has exploited VACNFs to provide a high surface area substrate and, therefore, larger fluorescent signals than would otherwise have been obtained using a conventional, planar geometry.[1] Trace analysis and DNA hybridization detection have also been demonstrated with VACNF electrodes that provided high signal-to-background ratio by exploiting the phenomenon of nonoverlapping electrochemical boundary layers.[2] Nanofiber arrays have also been incorporated as vertically oriented diffusion barriers in microfluidic devices to mimic cell functionality such as by isolating reagents within local regions of the fluidic platform.[3] The high aspect ratio and mechanical stability of VACNFs has also proved useful for the massively parallel delivery of molecular species, including DNA, to cells and tissue.[4]

Functionalization of VACNFs is a critical component in application of these high aspect ratio structures for practical devices. To display improved sensitivity to biomolecular recognition, it is paramount to achieve high surface coverage of the VACNFs with molecular receptor sites. Similarly, adequate functionalization with oligonucleotide probes is critical to generate an electrochemical hybridization detector with high sensitivity. For microfluidic devices featuring nanofibers as diffusion barriers, additional functionality can be achieved by surface modification of the VACNF barrier, for example, with active enzymes, electroactuated polymers, or pH responsive hydrogels. For DNA delivery applications, the method of binding and the physical location of DNA upon the nanofiber are likely critical elements in the success of delivery and likely even cell survival following cell/nanofiber interfacing.

To date, the bulk of nanofiber functionalization has been directed toward functionalization of the *entire* nanofiber surface. Chen et al. demonstrated, for example, that pyrrole may be electropolymerized as a conductive polymer film uniformly over the entire surface of nanofiber forest electrodes.[5] Lee et al. employed a diazonium-based methodology to functionalize the entire surface of VACNF electrodes with

* To whom correspondence should be addressed. E-mail: mcknightte@ornl.gov. Phone: 865-574-5681. Fax: 865-576-2813.
† Monolithic Systems Development Group, Oak Ridge National Laboratory.
‡ Molecular Scale Engineering and Nanoscale Technologies Research Group, Oak Ridge National Laboratory.
§ Lawrence University.
|| Earlham College.
⊥ University of Tennessee.
Biological and Nanoscale Systems Group, Oak Ridge National Laboratory.

(1) Baker, S. E.; Tse, K.-Y.; Hindin, E.; Nichols, B. M.; Clare, T. L.; Hamers, R. J. *Chem. Mater.* **2005**, *17*, 4971−4978.
(2) Koehne, J.; Li, J.; Cassell, A. M.; Chen, H.; Ye, Q.; Ng, H. T.; Han, J.; Meyyappan, M. *J. Mater. Chem.* **2004**, *14*, 676−684.
(3) Fletcher, B. L.; Hullander, E. D.; Melechko, A. V.; McKnight, T. E.; Klein, K. L.; Hensley, D. K.; Morrell, J. L.; Simpson, M. L.; Doktycz, M. J. *Nano Lett.* **2004**, *4* (10), 1809−1814.
(4) McKnight, T. E.; Melechko, A. V.; Hensley, D. K.; Griffin, G. D.; Mann, D.; Simpson, M. L. *Nano Lett.* **2004**, *4* (7), 1213−1219.

10.1021/cm052680g CCC: $33.50
Published on Web 06/09/2006

nitro groups that, in turn, could be electrochemically reduced to amino groups for the selective capture of oligonucleotide probes.[6] Fletcher demonstrated the interaction of nanofibers along their entire surface with a variety of fluorescently labeled species.[7] Demonstrations of gene delivery to cells were achieved by covalent attachment of plasmid DNA putatively along the entire length of arrays of nanofiber spikes.[8]

We anticipate that additional complexity of VACNF-based devices can be afforded by modification of these valuable strategies such that nanofibers can be functionalized in a *site-specific manner along the nanofiber length*. For example, gene delivery applications would likely be served by limiting the attachment of DNA to the extreme tips of nanofibers, rather than along the entire length of the nanofiber. In turn, microfluidic systems employing nanofiber barriers can be afforded an additional level of complexity by featuring modifications to the nanofibers only at discrete locations along their length, such that reactions or interactions might be limited only to these regions. Further, axial arrangements of materials can aid in defining pore regions in microfluidic barriers, can assist in co-localizing reagents, and can facilitate sealing of the nanofibers with lid structures of microfluidic manifolds.

In this manuscript, we document several approaches toward such site-specific functionalization along the nanofiber length including physical and electrochemical coating techniques, chemical immobilization of DNA and enzyme species, and covalent attachment of biotin followed by affinity-based capture of (strept)avidin-conjugated molecules. Each of these methods uses a common theme of employing sacrificial blocking layers of photoresist to limit the functionalization to unprotected, exposed regions of the nanofiber both along its length as well as at discrete locations across an array of nanofibers. Results of these approaches are explored using fluorescence and electron microscopy and quantum dot, fluorescent dye, and/or peroxidase assays to visualize and quantitate the functionalization of vertical nanofiber elements along their length with inorganic materials, molecular receptor sites, and active biological molecules.

Materials and Methods

Fabrication of Nanofiber Arrays. Arrays of VACNFs were fabricated as previously described.[9] In brief, 100 mm silicon wafers (n-type, ⟨100⟩) were spun with photoresist (SPR 955 CM 0.7) and patterned with 500 nm diameter holes on a 5 μm pitch using projection photolithography (GCA Autostep 200) and development (Microposit, CD26). A 30 s reactive ion etch (RIE; Trion Oracle, 150 Torr, 50 sccm oxygen, and 150 W of power) in oxygen plasma was used to remove residual resist from the developed regions. A Ni layer (50 nm) was deposited onto a wafer using electron-gun evaporation at 10^{-6} Torr. The excess metallization and photoresist was lifted off using a 1 h soak in acetone, followed by rinsing in a spray of acetone, followed by 2-propanol. VACNFs were then grown from the patterned Ni dots using direct current catalytic plasma enhanced chemical vapor deposition (C-PECVD).[9] Typically, nanofibers were grown to a length of approximately 7 μm with a conical shape featuring a tip diameter of <100 nm and a base diameter of 200−300 nm. Following synthesis, wafers were coated with a protective layer of photoresist (SPR 220 CM 7.0) and cut with a dicing saw into sized pieces. Prior to use, each piece was cleaned of the protective photoresist with a 30 min soak in acetone, followed by a rinse in acetone, 2-propanol, and water.

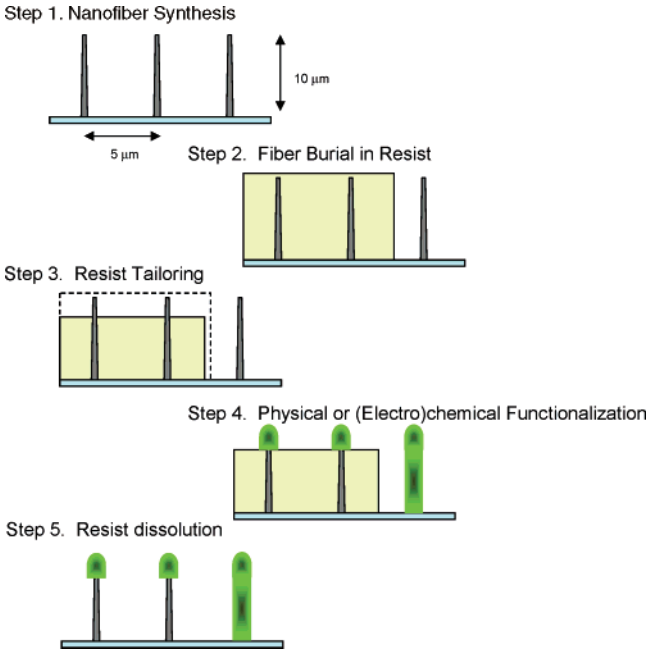

Figure 1. General scheme for photoresist-based blocking of chemical or electrochemical functionalization of arrays of VACNFs. Resist layers may be used to block functionalization sites specifically along the nanofiber height (two fibers depicted at the left of each drawing) or site specifically at different regions of an array (single fiber depicted at the right of each drawing.

Fabrication of Electrically Addressed Nanofiber Arrays. Arrays of VACNFs were fabricated on electrical interconnects as previously described.[10] In brief, 100 mm silicon wafers (n-type, ⟨100⟩) with 1 μm of thermal SiO_2 were metallized with 50 Å Ti/1000 Å W/50 Å Ti/100 Å Si using electron gun physical vapor deposition at 10^{-6} Torr. Patterned catalyst deposition and nanofiber synthesis was then performed as described in the previous subsection.

Photoresist-Based Protective Strategies for Height or Regional Specific Nanofiber Functionalization. The general scheme for photoresist-based protective strategies for nanofiber functionalization is presented in Figure 1. Nanofiber arrays are deterministically synthesized from photolithographically patterned thin films of Ni, which act as a catalyst for nanofiber growth in a DC-PECVD process (step 1). Following growth, nanofiber arrays are spun with photoresist which is then photolithographically patterned to expose (i.e., deprotect) regions of the substrate (step 2), similar to conventional lithography of planar substrates. In addition, however,

(5) Chen J. H.; Huang Z. P.; Wang D. Z.; Et al. *Synth. Met.* **2001**, *125* (3), 289−294.
(6) Lee, C.-S.; Baker, S. E.; Marcus, M. S.; Yang, W.; Eriksson, M. A.; Hamers, R. J. Electrically Addressable Biomolecular Functionalization of Carbon Nanotube and Carbon Nanofiber Electrodes. *Nano Lett.* **2004**, *4* (9), 1713−1716.
(7) Fletcher, B. L.; McKnight, T. E.; Melechko, A. V.; Simpson, M. L.; Doktycz, M. J. *Nanotechnology* **2006**, *17*, 2032−2039.
(8) McKnight, T. E.; Melechko, A. V.; Griffin, G. D.; Guillorn, M. A.; Merkulov, V. I.; Serna, F.; Hensley, D. K.; Doktycz, M. J.; Lowndes, D. H.; Simpson, M. L. *Nanotechnology* **2003**, *14* (5), 551−556.
(9) Melechko, A. V.; McKnight, T. E.; Hensley, D. K.; Guillorn, M. A.; Borisevich, A. Y.; Merkulov, V. I.; Lowndes, D. H.; Simpson, M. L. *Nanotechnology* **2003**, *14* (9), 1029−1035.
(10) McKnight, T. E.; Melechko, A. V.; Guillorn, M. A.; Merkulov, V. I.; Doktycz, M. J.; Culbertson, C. T.; Jacobson, S. C.; Lowndes, D. H.; Simpson, M. L. *J. Phys. Chem. B* **2003**, *107* (39), 10722−10728.

the vertical aspect of the nanofibers also allows specific heights of the vertical elements to emerge above an underlying photoresist layer. Oxygen RIE is then used to tailor the height of the photoresist protective layer, such that desired amounts of the nanofiber tips are exposed above the layer (step 3). These exposed regions can then be physically, chemically, or electrochemically functionalized (step 4), followed by removal of the blocking resist by chemical dissolution (step 5).

Chemical Functionalization of Nanofiber Arrays. Photoresist protected nanofiber arrays were chemically functionalized using previously reported methods of 1-ethyl-3-(3-diaminopropyl)carbodiimide (EDC) condensation of primary amine bearing molecules to carboxylic acid sites on the nanofibers.[8] Immobilized species included plasmid DNA, soybean peroxidase, gold-conjugated avidin, and biotin hydrazide. Common to each, a reaction buffer of 100 mM morpholinoethanesulfonic acid (MES) was brought to pH 4.8 with dropwise addition of 1 M NaOH. Plasmid DNA, soybean peroxidase, and gold-conjugated avidin were used at various dilutions in either phosphate buffered saline (PBS) or MES buffer. Biotin hydrazide was prepared as a stock solution of 50 mM biotin hydrazide in dimethyl sulfoxide (DMSO) that was sonicated for 30 s to aid dispersion. A total of 10 μL of the biotin hydrazide/DMSO solution was added to 1 mL of the 100 mM MES buffer, and the mixture was triturated extensively. For all reactions, 10 mg of EDC was added to 1 mL of the MES buffer, triturated, and subsequently added to the prepared solution of the diluted species to be immobilized. For example, for biotin hydrazide, each nanofiber array sample to be biotinylated was placed fiber-side-up in a flat-bottomed well of a 96-well plate, and 100 μL of the reaction mixture was placed on the chip. The plate was then covered with Parafilm and incubated for 34 h at room temperature on an orbital plate rocker ($\sim$30 rotations/min). The reaction mixture was aspirated from each well with a Pasteur pipet, taking care to not touch the fibered surface of the chip. Each well was then filled with a 10 mM Tris solution, incubated for 30 min to quench the EDC reaction, and aspirated. Each well was then rinsed in triplicate with distilled water. Similar treatments were conducted with DNA, soybean peroxidase, and gold-conjugated avidin but using either MES or PBS as opposed to DMSO for dilution and as the reaction buffer during the EDC condensation reaction.

Electrochemical Functionalization of Nanofiber Arrays. Photoresist protected electrically addressed nanofiber arrays were functionalized with polypyrrole via oxidation of 5 mM pyrrole monomer in acidic KCl (300 mM KCl/1 mM sulfuric acid) at the exposed carbon section of the nanofiber. Electropolymerization was conducted by wetting a small portion of the array defined by either an O-ring or an elastomeric well of poly(dimethylsiloxane) and connecting the electrically addressed array as the working electrode in a three-electrode configuration. The reference electrode in all experiments was Ag|AgCl (3 M KCl). A platinum coil with a surface area of greater than 10 times the active surface of the array was used as a counter electrode. Electropolymerization was conducted using multiple iterations of cyclic voltammetry between 0 V and 0.8 V versus Ag|AgCl (3 M KCl) at sweep rates of 500 mV/s.

Loss From Solution Assay for Quantification of Molecular Capture at Functionalization Sites. Biotinylation of nanofiber arrays and subsequent capture of molecular species was assessed by monitoring the capture and loss of a fluorescently conjugated streptavidin (fluorescein isothiocyanate-streptavidin, FITC-SA) from the solution above incubating nanofiber array chips. Biotinylated and non-biotinylated control chips were incubated at room temperature for 1 h in a 1X detector block (KPL) to reduce the potential for subsequent nonspecific binding. The chips were then extensively rinsed in distilled water and dried. The chips were then placed nanofiber-side-up in flat-bottomed wells of a 96-well plate, covered with 200 μL of solutions of FITC-SA in 500 mM NaCl, and incubated overnight at room temperature on an orbital rocker at 30 rotations/min. Following overnight incubation, the supernatant of each reaction well (three per sample type, including no chip, non-biotinylated chips, and biotinylated chips) was monitored for fluorescence (488 ex:520 em) in a microplate reader.

Peroxidase Assay for Quantification of Molecular Capture at Functionalization Sites. The number of species captured on biotinylated nanofiber arrays was also assessed by binding a peroxidase-conjugated avidin and subsequently monitoring the fluorescent reaction product of the bound peroxidase and the substrate, 3,3′,5,5′-tetramethylbenzidine. Biotinylated and non-biotinylated control chips were incubated at room temperature for 1 h in 1X detector block (KPL) to reduce the potential for subsequent nonspecific interactions. The chips were then extensively rinsed in distilled water and dried. The chips were then placed nanofiber-side-up in flat-bottomed wells of a 96-well plate, covered with 200 μL of a 5 ng/mL solution of peroxidase avidin (PA; Sigma) in distilled water, and incubated for 72 h at 4 °C. Following incubation, the chips were removed from the reaction solution, rinsed extensively in distilled water, and dried. One-half of the supernatant (100 μL) of each reaction well (3 per sample type, including no chip, non-biotinylated chips, and biotinylated chips) was mixed with an equal volume (100 μL) of the Sureblue Peroxidase Assay solution (KPL). Each chip was also covered with 100 μL of distilled water and an equal volume (100 μL) of the Sureblue Peroxidase Assay solution. Following 300 s of reaction at room temperature, each reaction was stopped with 100 μL of 1 M HCl, and the solution was monitored via absorbance at 430 nm in a microplate reader. Results were compared against a triplicate set of standard solutions of PA (5, 2.5, 1.25, 0.625, 0.3, 0.15, 0.075, 0.0325 ng/mL) in distilled water that were mixed and incubated in parallel with the chip samples. It should be noted that these incubations and assays were conducted in distilled water, as opposed to high salt solutions (>500 mM NaCl). Initial attempts at binding in high salt resulted in loss of activity of the PA.

Results and Discussion

Photoresists as Blocking Agents for Biochemical Functionalization. Photoresist methods have been established as ubiquitous processing steps in microfabrication. Conventionally, photoresists provide a protective mask for subsequent *materials* processing steps including predominantly wet and dry etching. However, they may also be exploited as masks to direct the *biochemical functionalization* of devices, provided the chemistries of subsequent photoresist removal following the functionalization do not substantially impact the activity or reactivity of the immobilized biological species. Photoresist may be removed using a variety of processes, including oxygen RIE, development following exposure in aqueous base, or dissolution in organic solvents, such as acetone and isopropyl alcohol. When using photoresists as a mask for biochemical functionalization, such as for the patterned tethering of DNA or enzymes, selection of the removal process will largely be governed by the chemical tolerances of the species being immobilized. Double stranded DNA, for example, can denature under basic conditions, resulting in the potential loss of a nontethered complementary strand and possible reduction or elimination of the template's transcriptional activity. As such, aqueous base removal of

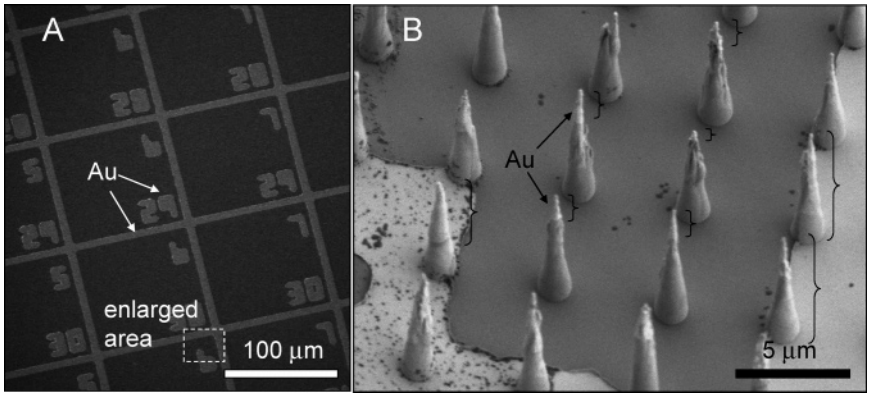

Figure 2. Photoresist-based regional blocking of physical functionalization of a nanofiber array. Following protection and tailoring, as presented in Figure 1, titanium and gold were physical vapor deposited onto the unprotected regions of a nanofiber array. Fibers within the 100 μm square grids received titanium and gold only on the tips emergent from the protective photoresist. Fibers in regions where photoresist was exposed and removed were metallized along their entire length.

photoresist can be problematic. Acetone and isopropyl or ethyl alcohols, on the other hand, are routinely used with DNA isolation and purification and will dehydrate tethered DNA but will not significantly impact its transcriptional activity upon subsequent rehydration. Similarly, many enzymes will retain activity following a period of solvent dehydration. Acetone has often been used as the solvent of choice for tissue dehydration in histological pathology as a result of the ability of enzymatic activity to be largely recovered following rehydration.[11−13] As such, with respect to the materials being tethered and their maintained activity, photoresist strategies are plausible as a means of patterning biochemical immobilizations.

The ease of patterning photoresists via photolithography provides a means of blocking and exposing sites spatially across a planar substrate. Further, the ability to tailor the depth of photoresist layers either via the choice of photoresist viscosities or spin speeds or by subsequent etch processes enables the deterministic blocking or exposure of specific lengths (heights) of nonplanar features, such as high aspect ratio nanofibers. The survival of vertically aligned nanofibers to spins of various resists was first documented by Guillorn[14] and subsequently has provided the basis for use of this ubiquitous processing step in the microfabrication of a variety of nanofiber-based devices.[3,10,14] Guillorn demonstrated that not only could nanofibers survive the process of being spun with resists, but they could also withstand subsequent photoresist processing steps including exposure, development, oxygen RIE, and acetone/2-propanol photoresist dissolution. In lithographically exposed regions of a nanofiber-based device, photoresist could be developed away, leaving little if any residue on the nanofiber surfaces within these regions. Further, residual resist could be removed by a "descumming" process of brief exposure (30 s) to oxygen plasma. In addition, even when nanofibers were buried in resist, oxygen plasma could be used to controllably expose the underlying nanofibers by preferential etching. As such, photoresist lithography and dry etch processing can be used to deterministically expose specific *regions* of nanofibers on a substrate in addition to specific *lengths* of nanofibers above a blocking layer of photoresist.

Photoresist-Based Regional and Height-Specific *Physical* Functionalization. Regional and height-specific *physical* functionalization of an array of VACNFs using this photoresist protective approach (overviewed in Figure 1) is demonstrated in Figure 2. Here, nanofiber arrays at 5 μm pitch were spun with a 6 μm thick layer of photoresist. This resist layer was then lithographically patterned to expose gridlines in the resist at 100 μm intervals in addition to exposing numerical indices within each 100 μm square region. Following exposure and development of the resist from exposed regions, a 30 s oxygen plasma etch was used to clean residual resist from the gridlines and to remove residual resist from the emergent tips of the nanofibers. This provided 100 μm square regions where nanofiber bases were blocked with resist while their tips were emergent above the resist layer. Each of these regions was surrounded by a 5 μm wide gridline where the resist was completely removed, such that nanofibers in these regions were completely unprotected by resist. Nanofibers were similarly unprotected in the numerical index locations, as a result of exposure and resist removal in these areas. Following this resist tailoring, the structure was physically coated with 100 Å Ti and 500 Å Au using electron gun physical vapor deposition. Following this metallization, the blocking resist layer and excess Ti/Au was removed by dissolution of the resist in acetone. The resulting structure demonstrates tip selective metallization of the nanofibers within the 100 μm square grids, surrounded by fully metallized nanofibers in the peripheral gridlines and within numerical index regions. It can be observed that the dimension of spatial selectivity between metallized and unmetallized regions is better than 5 μm using resist burial of approximately 6 μm thickness.

Photoresist-Based Regional and Height-Specific *Chemical* Functionalization. Regional *chemical* functionalization of a nanofiber array using this tailored resist approach is demonstrated in Figure 3. Following synthesis, a nanofiber

(11) Barrow, B. J.; O'Riordan, M. A.; Stellato, T. A.; Calkins, B. M.; Pretlow, T. P. *Cancer Res.* **1990**, *50*, 1911−1916.
(12) Pretlow, T. P.; O'Riordan, M. A.; Kolman, M. F.; Jurcisek, J. A. *Am. J. Pathol.* **1990**, *136*, 13−16.
(13) Beckstead, J. H.; Halverson, P. S.; Ries, C. A.; Bainton, D. F. *Blood* **1981**, *57*, 1088−1098.
(14) Guillorn, M. A.; McKnight, T. E.; Melechko, A. V.; Austin, D. W.; Merkulov, V. I.; Simpson, M. L.; Lowndes, D. H. *J. Appl. Phys.* **2002**. *91*, 3824−3828.

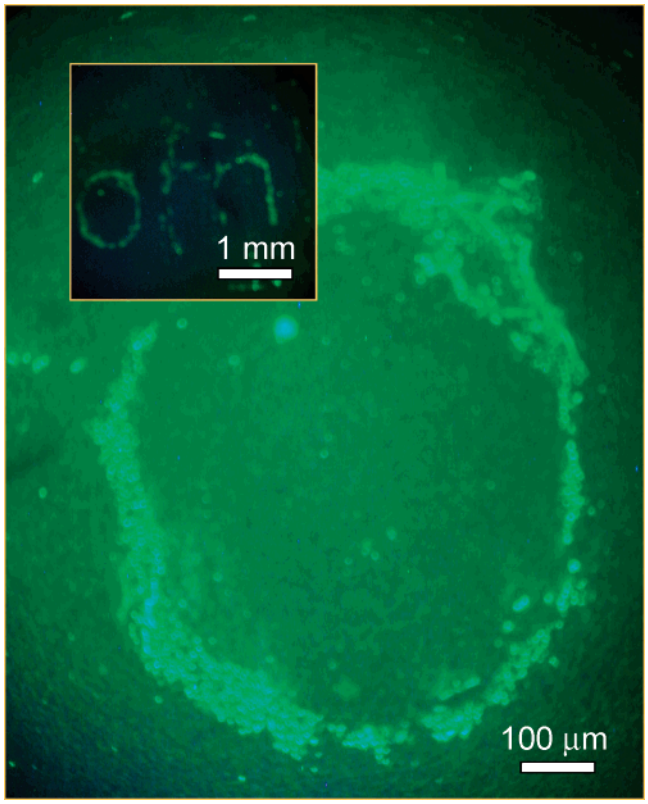

Figure 3. Photoresist-based regional blocking of chemical functionalization of a nanofiber array. DNA, as visualized via fluorescent imaging after intercalation of a dye, was covalently tethered using a carbodiimide mediated chemistry only to regions free of photoresist. Each small dot in the image corresponds to individual nanofiber elements.

array was buried in a spun layer of photoresist that was photolithographically patterned with the letters "ornl" using a mask generated on transparency film printed using a laser printer at 1100 dpi. Following development and an oxygen plasma etch, nanofibers within the lettered regions of the substrate were accessible for subsequent derivitizations while those under the photoresist were blocked. As such, during an overnight condensation reaction with 100 ng of a 5081 bp plasmid DNA (in 100 mM MES buffer with 10 mg/mL 1,1-ethyldiaminopropylcarbodiimide) only the exposed nanofibers were able to covalently tether the DNA template, putatively due to a condensation reaction between DNA base amines and carboxylic acid sites on the exposed nanofibers. Following acetone liftoff of the protective photoresist layer, only the exposed regions of the device hosted the tethered plasmid, as evidenced by fluorescent microscopy following labeling with a DNA intercalating dye (Picogreen, Molecular Probes, Eugene, OR).

To facilitate directed chemical or electrochemical functionalization *limited to nanofiber tips*, the base of a nanofiber array sample was protected in a layer of photoresist (for example, SPR220 CM 7.0) while nanofiber tips remained emergent above the protective resist layer. The thickness of this photoresist was selected by appropriate spin rate and viscosity to keep tips exposed above the photoresist surface. To adjust the amount of emergent nanofiber length, the photoresist was etched back using oxygen RIE. Chemical functionalization was then conducted on all emergent surfaces, followed by a removal of the protective photoresist layer by acetone dissolution.

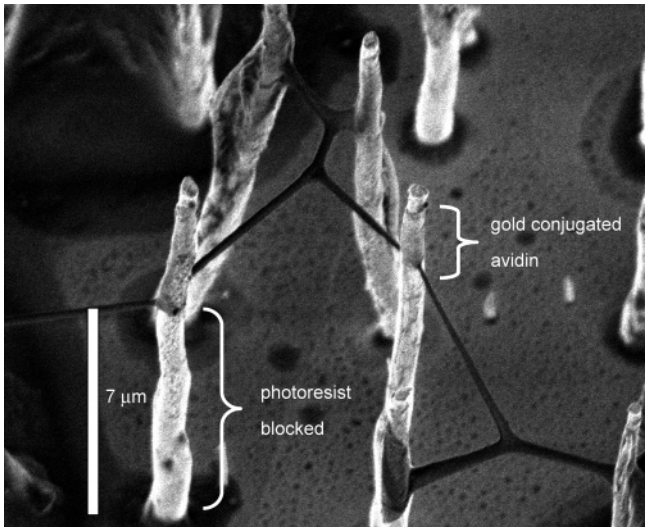

Figure 4. Covalent coupling of gold-conjugated avidin to the tips of nanofibers using an underlying blocking layer of photoresist. This image was captured after acetone based removal of the photoresist blocking layer.

Table 1. Measurement of the Amount of Exposed Nanofiber Tip versus Protected Base Related to the Etch Time Used To Tailor the Height of a Blocking Layer of Photoresist[a]

etch time (sec)	functionalized tip length (μm)	protected base length (μm)
60	1.5 ± 0.5	9.1 ± 0.3
120	2.0 ± 0.2	8.0 ± 0.3
300	4.5 ± 0.8	6.6 ± 0.1

[a] Functionalized lengths were determined by scanning electron microscopy of gold−avidin conjugated to the nanofiber tips.

Functionalization of exposed nanofiber tips is demonstrated in Figure 4. An array of 10−12 μm tall nanofibers was spun with an ~7 μm layer of photoresist and soft-baked at 120 °C for 90 s, leaving the upper ~5 μm of the fibers exposed. Following softbake of the unexposed resist, a 30 s oxygen plasma "descum" was used to remove residual resist from the nanofiber tips. The samples were then immersed into a solution of 100 mM MES buffer, 10 mg/mL EDC, and 10 μg/mL gold-conjugated avidin (KPL) wherein available primary amines of the avidin (N-termini or available lysine residues) could either react with carboxylic acid sites on fibers or could cross-link with other avidin molecules. Following overnight reaction, the chips were rinsed in MES buffer and water and dried. The protective photoresist layer was then removed by immersion in acetone followed by rinsing in a spray of isopropyl alcohol. The result was imaged at 1 kV in a Hitachi 4700 scanning electron microscope. As evidenced by Figure 4, the cross-linking of gold-conjugated avidin was limited to the upper portion of the nanofibers, with the underlying base of the nanofibers being protected by the photoresist from participating in the condensation reaction.

Using the same procedure but etching back the protective photoresist layer with an oxygen plasma prior to the functionalization reaction provides a mechanism for controlling the length of the functionalization along the nanofiber tip. Table 1 provides an overview of the lengths of functionalized tips and of protected bases for an array of ~12 μm tall fibers following spin coating with ~10 μm of photoresist and variable etch times in an oxygen RIE (250

mTorr, 150 W, 50 sccm O_2). Measurements of these lengths were conducted following the functionalization reaction using scanning electron microscopy (as in Figure 4) to determine the lengths of tip regions of nanofibers coated with gold-conjugated avidin and the lengths of the underlying base regions free of this surface modification. Functionalized tip length in these data corresponds to the emergent height of nanofiber above the protective photoresist layer and is, therefore, significantly influenced by variation in overall nanofiber length (~10−20%). In contrast, the *protected* base length was a much more reproducible value, as a result of the relative uniformity in the etched protective resist layer thickness. Using these data, the etch rate of the photoresist and, therefore, the deprotect rate of the fiber tip were determined to be ~600 nm/min of oxygen etch. This provides a resolution of approximately 100 nm in the ability to tailor the protective resist height, based upon a minimum etch time of approximately 10 s. Variation in etch parameters, such as plasma pressure and power, however, can likely provide increased resolution of the resist tailoring process if necessary.

It should be noted that, during the resist etch, the nickel particle normally present at the nanofiber tip is required to protect the structure of the underlying nanofiber from the oxygen plasma etch. If this particle is removed, the nanofibers will experience some etching in the oxygen plasma, albeit at a much slower etch rate (~25−100 nm/min)[15] than the photoresist (average ~600 nm/min). Additionally, it is noted that the extreme tips of most nanofibers are void of the gold-conjugated avidin, a phenomenon visible on the tips of nanofibers in Figure 4. This region corresponds to the location of the nickel catalyst which resides at the nanofiber tip throughout growth. Exposure of this region to the resist-tailoring oxygen plasma etch may remove the carbon layer from the nickel particle and may, therefore, eliminate any carboxylic acid groups and subsequent EDC mediated binding of the gold-conjugated avidin in this region.

Photoresist-Based Regional and Height-Specific *Electrochemical* Functionalization. In addition to serving as a protective barrier during chemical functionalization, photoresist may also be used in the same capacity during electrochemical functionalization, including electropolymerization and electrodeposition. For example, the electropolymerization of pyrrole onto electrodes to form conductive polymer films has frequently been used in the development of redox mediating polymer films,[16] electroactuators based upon dopant inclusion and expulsion,[17] and electrically addressable tissue scaffolds.[18] The electropolymerization of pyrrole onto nanofiber and nanotube arrays has been demonstrated to form relatively conformal coatings along the entire length of a nanofiber.[5] However, using similar photoresist protective schemes as described for chemical derivitization, this electropolymerization can be limited to discrete regions of a wafer and to the tips of fibers exposed above a resist blocking layer.

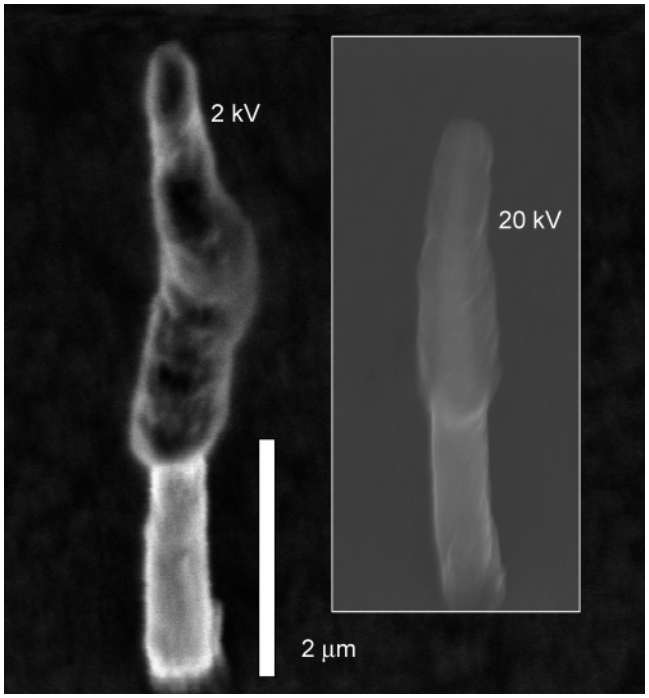

Figure 5. Electropolymerization of pyrrole to the emergent tips of nanofibers protected under a base layer of photoresist. In this image, the photoresist blocking layer has been removed by acetone dissolution following the polymerization.

Figure 5 presents the results of electrochemical functionalization (i.e., pyrrole electropolymerization) on a nanofiber array that was partially buried beneath approximately 2 μm of SPR 220 CM3.0 photoresist. It should be noted that, upon exposure, this photoresist develops and, therefore, dissolves in aqueous base. As such, application of photoresist for this approach requires maintaining an acidic environment during the electropolymerization of the polymer film, so as not to unintentionally remove the blocking photoresist during the electrochemical reaction. Initial attempts at polymerization in PBS or unbuffered KCl resulted in dissolution of the protective photoresist layer around the nanofiber electrodes. This dissolution was eliminated upon the addition of 1 mM sulfuric acid to the pyrrole solution. It is anticipated that acidic buffers would also prove effective for preserving the blocking photoresist layer during electropolymerization.

Two-Step Functionalization of Nanofiber Arrays Via Biotinylation. A limitation of many direct functionalization strategies, such as the direct immobilization of (strept)avidin to nanofibers or the electropolymerization of pyrrole, is that the thickness of the immobilized layer may be difficult to control. (Strept)avidin, for example, may cross-link in solution and upon the functionalized surface thereby generating a thick coating on the nanofiber. Polypyrrole also will grow radially from the nanofiber, dependent upon polymerization time, monomer concentration, and local formation and capture of pyrrole dimers and oligos. An example of such "uncontrolled" growth is demonstrated in the avidin−gold conjugation of Figure 4, where "webbing" of material between nanofibers is observed in addition to immobilization to nanofibers. This "webbing" of material may be the result

(15) Melechko, A. V.; McKnight, T. E.; Guillorn, M. A.; Austin, D. W.; Ilic, B.; Merkulov, V. I.; Doktycz, M. J.; Lowndes, D. H.; Simpson, M. L. *J. Vac. Sci. Technol., B* **2002**, *20* (6) 2730−2733.
(16) Barisci, J. N.; Conn, C.; Wallace, G. G. *Trends Polym. Sci.* **1996**, *4* (9), 307−311.
(17) Smela, E. *Adv. Mater.* **2003**, *15* (6), 481−494.
(18) Schmidt, C. E.; Shastri, V. R.; Vacanti, J. P.; Langer, R. *Proc. Natl. Acad. Sci. U.S.A.* **1997**, *94*, 8948−8953.

of extensive cross-linking of the gold-conjugated avidin with itself, generating a thick immobilized layer of the material rather than a discrete monolayer coverage. This webbing behavior may also be driven by the potential for the condensation reaction to occur between the avidin and carboxylic acid sites formed on the resist layer surface during the back-etch of this layer with oxygen plasma. Indeed, high concentrations of the gold−avidin during the EDC reaction were found to fully cover regions of the photoresist layer, making subsequent dissolution of this layer in acetone difficult. This cross-linking phenomenon is typically not desirable when discrete functionalization of only nanofiber tips is required or when monolayer coverage of a species is desired. In this scenario, it can be advantageous to use an indirect, two-step functionalization chemistry, where the resist protected nanofibers are first modified with a specific ligand that is unable to cross-link. Following the deprotection via resist liftoff, only specific sites will be functionalized with this ligand, and a subsequent capture of a receptor species can be limited to these sites. The biotin/avidin affinity system is an excellent candidate for such a stepwise functionalization. Biotin hydrazide may be used in an EDC-mediated condensation reaction to biotinylate nanofiber arrays in a photoresist-protected site-specific manner. During this condensation, there is no risk of the species (biotin hydrazide) cross-linking with itself, and unwanted immobilization to the photoresist surface can be eliminated during the photoresist liftoff. Following photoresist removal, biotinylated regions of the device can be used for affinity capture of (strept)avidin species or to capture the wide assortment of commercially available (strept)avidin-conjugated dyes and enzymes.

To evaluate the potential of this stepwise functionalization, a set of nanofiber arrays was first protected by spotting the center of each chip with a pipet dispensed droplet of approximately 5 μL of SPR220 CM7.0 photoresist. Following stepwise softbake at 90 °C for 5 min and 120 °C for 3 min, the samples were then biotinylated overnight using biotin hydrazide, MES buffer, and EDC as detailed in Materials and Methods. Following the overnight reaction, the samples were extensively rinsed, and the photoresist protective layer was removed from each via soaking in acetone and rinsing in acetone and isopropyl alcohol. This putatively provided a region at the center of each chip that was biotin-free, surrounded by a biotinylated periphery. To verify this, observations of biotin coverage on chips and the functionality of these sites for (strept)avidin capture were conducted by incubating chips with a variety of fluorescent avidin and/or streptavidin conjugates and imaging these chips with a fluorescent microscope. During this imaging, and consistent with earlier published images,[8] nanofiber arrays were found to exhibit significant background fluorescence, with 488 nm excitation resulting in bright yellow dots at nanofiber locations and 514 nm excitation generating red emission from the fiber array. This broad native fluorescence from the nanofiber array confounded attempts to definitively distinguish the capture of conventionally conjugated (strept)-avidins (FITC-SA and tetramethyl rhodamine-avidin, TMR-avidin) versus the indigenous fluorescence of the nanofiber

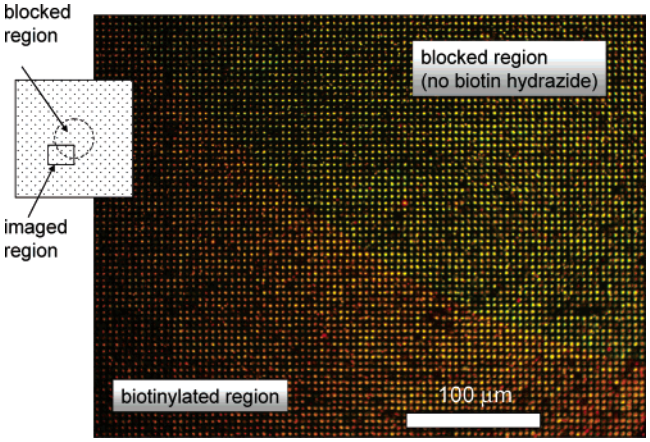

Figure 6. Fluorescent micrograph (488 nm excitation, 520−650 emission) of the interface between biotinylated and non-biotinylated regions of a nanofiber array following incubation with streptavidin-conjugated 655 nm emitting quantum dots. In regions with biotin, capture of the streptavidin-conjugated quantum dots is demonstrated by the 655 nm emission of the quantum dot. In the photoresist blocked region, where there is no biotin, considerably less Qdot SA was captured and the native fluorescence of the fibers is evident (~530 emission from 488 excitation).

array, even when employing chips that had been blocked during biotinylation to provide a discrete interface between regions that should and should not capture the conjugated avidins. Successful imaging, however, was achieved using streptavidin-modified quantum dots, specifically Quantum Dot Streptavidin Conjugate 655, Qdot Corp. The fluorescent shift of these quantum dots (488 excitation, 655 emission) was significantly larger than the fluorescence shift of the nanofiber array. Therefore, using a widepass emission filter with a 488 excitation, the red emission of the 655 Qdot could clearly be distinguished against the native yellow (520−550 nm) emission of the nanofiber array. Figure 6 provides a fluorescent micrograph of the interface between a biotinylated and non-biotinylated region of a nanofiber array following incubation with Qdot-SA-655 and rinsing in distilled water. Across the array, nanofibers are visible as yellow spots at regular intervals corresponding to the interfiber spacing of 5 μm. Discrete red dots corresponding to the presence of the Qdot-SA-655 are also visible across the array, predominantly in the lower left of the image. This region of the fiber array corresponds to a portion of the biotinylated periphery of the sample, and resultant Qdot SA capture clearly demonstrates the functionality of the tethered biotin for avidin capture. In contrast, the upper right region of this image was blocked with the SPR220 photoresist layer during biotinylation and, therefore, presents only the native fiber surface during avidin incubation and capture. While nonspecific binding of the streptavidin Qdots does occur across the array, in general this is at a level much lower than the specific capture in biotinylated regions.

In addition to fluorescent microscopy, scanning electron microscopy was used to ascertain the physical location of capture of the streptavidin-conjugated quantum dots upon nanofiber arrays and, therefore, to determine the physical location of biotinylation. Figure 7 is composed of scanning electron micrographs of a putatively biotinylated nanofiber following capture of Qdot-SA-655. At 30 kV acceleration voltage, the inorganic quantum dots can clearly be distin-

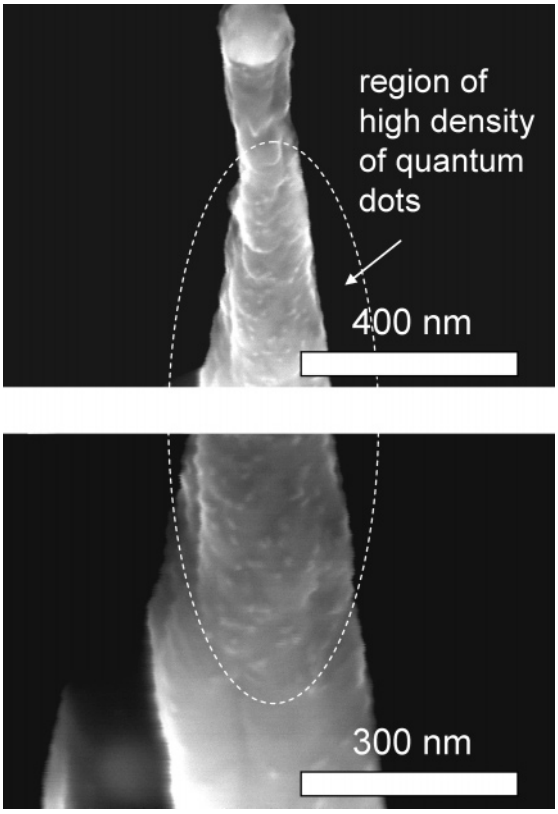

Figure 7. Scanning electron micrographs of streptavidin-conjugated quantum dots after binding to putative biotin sites on a nanofiber array. Quantum dots could be found everywhere throughout the sample, including on the substrate and on the vertically aligned nanofibers. In general, the density of quantum dots appeared higher in a region within approximately 30−90% of the fiber height. Note, merging of images is not intended to imply a contiguous region of the nanofiber but rather to exemplify differences of avidin capture at the midsection versus at the tip and base.

guished as small (∼20 nm) white dots on the surface of the nanofibers. In general, without using photoresist blocking strategies, quantum dots were found on samples on both nanofibers and interfiber locations of the underlying substrates. By using photoresist strategies to block the underlying substrate during biotinylation, however, the presence of streptavidin-conjugated quantum dots could be largely limited to only the emergent portions of the nanofibers.

Quantification of Molecular Capture at Functionalization Sites via Loss from Solution Assay. To provide a quantitative measure of the number of avidin molecules captured at sites available on a biotinylated nanofiber array, "loss from solution" assays were conducted following incubation of biotinylated and non-biotinylated chips in solutions of FITC-conjugated streptavidin at various dilutions. On the basis of coverage data from scanning electron micrographs of quantum dot capture on biotinylated fibers (∼500 quantum dots/μm^2 in the regions of high capture), initial incubations were conducted in a FITC-SA solution containing approximately the number of molecules necessary to saturate the biotin sites on the nanofibers of a 2.3 mm square nanofiber array. This was estimated to be approximately 0.2 ng/chip, based upon the number of nanofibers per chip (∼210 000), the approximate surface area of each nanofiber (15 μm^2), and the molecular weight of FITC-SA (∼60 kDa). Table 2 presents the fluorescence induced response (FIR) of the supernatant from triplicate samples of

Table 2. FIR of FITC−Streptavidin Remaining in Solution after Overnight Incubation of Biotinylated and Non-Biotinylated Nanofibered Substrates in 200 μL of 1.0 ng/mL FITC-SA in 500 mM NaCl[a]

background count of FITC-SA-free solution	46 000 ± 900
count from 0.2 ng of FITC-SA solution	51 000 ± 700
count from solution above non-biotinylated chips	50 500 ± 600
count from solution above biotinylated chips	46 200 ± 100

[a] Non-biotinylated samples removed very little FITC-SA from the solution. In contrast, biotinylated samples appear to have removed all the FITC-SA from the incubation volume.

biotinylated and non-biotinylated chips following overnight incubation in 0.2 ng/200 μL of FITC-SA in 500 mM NaCl. Triplicate samples of the FITC-SA solution and a neat solution of 500 mM NaCl were also processed in parallel to the chip incubations to account for any loss of the FITC-SA to the reaction reservoir surfaces. As evident from these data, overnight incubation resulted in almost complete removal of the FITC-SA by the biotinylated chips from the supernatant, presumably as a result of capture of the conjugated streptavidin at biotin sites on the nanofiber array. In contrast, the non-biotinylated samples did not remove appreciable amounts of FITC-SA from their reaction volumes. Following incubation and measurement of the first 0.2 ng/chip, subsequent incubations in additional FITC-SA resulted in no additional measurable "loss from solution" of this fluorescently conjugated streptavidin, indicating that the available avidin binding sites were saturated during the first round of incubation. Note, however, that the fluorescent measurement was close to the background limit of the plate reader. As such, this estimation of biotin coverage via FITC-SA capture can only be considered a rough approximation. Nonetheless, the result correlates well with earlier observations with quantum dots.

Quantification of Molecular Capture at Functionalization Sites via Peroxidase Assay. To provide a more sensitive measure of available avidin capture sites, an enzyme reporter system was employed that could provide chemical amplification of the fluorescent measurement by turning over a large number of enzyme substrates for each active enzyme within the system. Using PA in place of FITC-SA, each active enzyme unit could react with many molecules of a nonfluorescent substrate, 3,3′,5,5′-tetramethylbenzidine (TMB), to generate many molecules of a fluorescent product. Furthermore, as a solution-based assay, this approach could be used to quantify both the loss of PA from a solution above a nanofiber chip as well as the presence of active PA on the chip following the immobilization reaction, without interference from the native fluorescence of the chip.

Table 3 presents the peroxidase activity of both the incubation solution from above nanofibered substrates and the substrates themselves following a 72 h incubation in 1 ng of PA in 200 μL of distilled water. One-half of the incubation solution was assayed and compared to a triplicate set of PA dilutions for calibration. The non-biotinylated control samples appear to have pulled approximately 0.2 ng of PA from the 1/2 volume sample (0.4 ng from the total volume), whereas the biotinylated chips pulled approximately 0.25 ng of PA from the solution (0.5 from the total volume). In turn, the control samples demonstrated near-baseline

Table 3. Assay of Peroxidase Activity of Both the Incubation Solution above the Samples (Supernatant) after 72 h and the Nanofiber Array Samples (On-Chip)[a]

	supernatant (ng of PA-A)	on-chip (ng of PA-A)
well without chip	0.56 ± 0.03	
non-biotinylated chips	0.36 ± 0.01	0.02 ± 0.02
biotinylated chips	0.28 ± 0.07	0.11 ± 0.00

[a] Although both the biotinylated and the non-biotinylated samples appear to have removed PA from the solution, only the biotinylated samples show any appreciable peroxidase activity.

peroxidase activity, whereas the biotinylated samples generated a TMB fluorescent product equivalent to approximately 0.1 ng of PA. Discrepancies between the amount removed from the incubation solution and the amount on samples may be due to nonspecifically adsorbed PA that was subsequently removed during rinse steps prior to the assay. Bound PA may also experience a reduction in activity due to immobilization. Nonetheless, these values are consistent with both the FITC-SA loss from the solution assay as well as approximation of biotin coverage based on scanning electron microscopy of streptavidin-conjugated quantum dots.

Conclusion

There are many approaches available for the chemical and electrochemical functionalization of VACNF devices. In this work, strategies were developed that enable many of these functionalization approaches to be applied such that modification is obtained in a site-specific manner along the nanofiber length. Flexible and convenient photoresist techniques were demonstrated that provide site-specific physical, chemical, and electrochemical functionalization of unprotected, exposed regions of the nanofiber both along its length as well as at discrete locations across an array of nanofibers. The resolution of regional patterning using these techniques is determined by the photoresist patterning resolution, which was demonstrated to be less than 5 μm using contact lithography. Vertical resolution, achieved by tailoring the height of a protective photoresist layer using oxygen plasma etching, approaches $\sim$100 nm. These strategies can be employed for direct physical, chemical, and electrochemical functionalization, demonstrated in this effort via physical vapor deposition of gold, direct covalent attachment of plasmid DNA and gold-conjugated avidin, and surface biotinylation followed by capture of active enzyme-conjugated avidins. It is anticipated that the ease of use and flexibility of these site-specific strategies can be applied for a variety of functionalization chemistries and will assist in enabling additional levels of complexity in nanofiber-based devices for applications including gene delivery, microfluidics, and nanostructured biosensors.

Acknowledgment. The authors wish to thank P.H. Fleming for assistance with metal depositions and D. Hensley for fiber synthesis. This work was supported in part by the National Institute for Biomedical Imaging and Bioengineering under assignments 1-R01EB006316 (T.E.M.) and 1-R01EB000657 (M.J.D.) and through the Laboratory Directed Research and Development funding program of the Oak Ridge National Laboratory, which is managed for the U.S. Department of Energy by UT-Battelle, LLC. C.P. and S.W.J. participated in the Higher Education Research Experiences (HERE) and Science Undergraduate Laboratory Internships (SULI) programs, respectively. A.V.M. and M.L.S. acknowledge support from the Material Sciences and Engineering Division Program of the DOE Office of Science. A portion of this research was conducted at the Center for Nanophase Materials Sciences, which is sponsored at Oak Ridge National Laboratory by the Division of Scientific User Facilities, U.S. Department of Energy.

CM052680G